

Synthesis and Evaluation of Graphene Aerogel-Supported $\text{Mn}_x\text{Fe}_{3-x}\text{O}_4$ for Oxygen Reduction in Urea/ O_2 Fuel Cells

Keyru Serbara Bejigo,^[a] Bang Ju Park,^[b] Ji Hyeon Kim,^[a] and Hyon Hee Yoon^{*[a]}

Graphene aerogel-supported manganese ferrite ($\text{Mn}_x\text{Fe}_{3-x}\text{O}_4/\text{GAs}$) and reduced-graphene oxide/manganese ferrite composite ($\text{MnFe}_2\text{O}_4/\text{rGO}$) were synthesized and studied as cathode catalysts for oxygen reduction reactions in urea/ O_2 fuel cells. $\text{MnFe}_2\text{O}_4/\text{GAs}$ exhibited a 3D framework with a continuous macroporous structure. Among the investigated Fe/Mn ratios, the more positive oxygen reduction onset potential was observed with Fe/Mn = 2/1. The half-wave potential of $\text{MnFe}_2\text{O}_4/\text{GAs}$ was considerably more positive than that of

$\text{MnFe}_2\text{O}_4/\text{rGO}$ and comparable with that of Pt/C, while the stability of $\text{MnFe}_2\text{O}_4/\text{GAs}$ significantly higher than that of Pt/C. The best urea/ O_2 fuel cell performance was also observed with the $\text{MnFe}_2\text{O}_4/\text{GAs}$. The $\text{MnFe}_2\text{O}_4/\text{GAs}$ exhibited an OCV of 0.713 V and a maximum power density of 1.7 mW cm^{-2} at 60 °C. Thus, this work shows that 3D structured graphene aerogel-supported MnFe_2O_4 catalysts can be used as an efficient cathode material for alkaline fuel cells.

1. Introduction

Recently, anion exchange membrane fuel cells (AEMFCs) have received considerable attention in area of fuel technology with promising output. AEMFCs have benefits over proton exchange membrane fuel cells (PEMFCs) as operated in alkaline media, which boosts oxygen reduction kinetics and allows the use of non-precious metal catalysts.^[1] Other benefits of AEMFCs are lower fuel cross-over due to the movement of anions against fuel and fuel flexibility,^[2] various fuels such as H_2 , methanol, ethanol, and glucose can be used in AEMFCs. Urea ($\text{CO}(\text{NH}_2)_2$), is an industrial product mainly used as an agricultural fertilizer, can also be used as a fuel in AEMFCs. Urea is a non-toxic, non-flammable, and biodegradable compound, and is relatively cheap and convenient to store and transport compared with hydrogen.^[3] Furthermore, urine and urea-containing wastes can be purified with electricity generation using AEMFCs.

In AEMFCs, anode reaction oxidizes the fuel with the release of electrons, which pass through an external circuit, while the electrolyte membrane allows the transfer of OH^- produced from the oxygen reduction reaction (ORR) at the cathode.^[4] ORR is known to be multifaceted owing to its multistep and multi-electron transfer behavior involving numerous adsorption/desorption stages for oxygen-containing species such as O , O_2^- ,

OH , HO_2^- , and H_2O_2 as reaction intermediates, which makes it slower.^[5,6] Currently, Pt is the most active ORR catalyst. However, its high cost is a critical barrier for practical implementation. To reduce Pt consumption, it has been alloyed with non-precious metals such as Co, Cr, and Ni, which are reported to be efficient catalyst for ORR.^[7] As an alternative to Pt, non-noble catalysts for ORR including transition metal oxides,^[8] transition metal nitrides,^[9] and their chalcogenides^[10] have been studied and reported as promising catalysts for ORR. Among the new approaches, oxides of transition metals exhibited outstanding performance for ORR.^[11] For instance, manganese ferrite (MnFe_2O_4), which has an inverse spinel structure with multiple valance electrons, has been proved to be a good ORR catalyst in alkaline media. Zhu and coworkers also reported that manganese-substituted ferrite outperformed over others (Cu- and Co-substituted ferrite) and was even comparable to Pt in basic media.^[12] However, MnFe_2O_4 is a semi-conductive material that leads to insufficient performance resulting from poor ion and electron transfer.^[13] The catalytic activity of MnFe_2O_4 was improved by integrating it with other materials that are capable of boosting conductivity in addition to the reduction in agglomeration of active catalyst. MnFe_2O_4 -supported conductive materials such as graphene and polyaniline composites were studied for ORR and exhibited higher catalytic activity than MnFe_2O_4 did.^[14]

Graphene is one of the carbon-based nanomaterials with a high electrical conductivity, large surface area, and good mechanical strength, which make it an ideal support for catalyst materials. Incorporating metal and their oxide nanoparticles into graphene creates porous networks that enhance both catalyst activity and its stability.^[15,16] Graphene-supported transition metal oxides such as MnCo_2O_4 and Mn_3O_4 nanoparticles exhibited good ORR performance in alkaline media.^[17,18] Recently, graphene aerogel having a three-dimensional mesoporous structure has attracted the most attention owing to its high surface area, light weight, and high porosity, which allow sufficient electron transfer pathways.^[19–21] Wang et al. developed

[a] K. S. Bejigo, Prof. J. H. Kim, Prof. H. H. Yoon
Department of Chemical and Biological Engineering
Gachon University
1342 Seongnam-daro, Seongnam, S. Korea
E-mail: hhyoon@gachon.ac.kr

[b] Prof. B. J. Park
Department of Electronic Engineering
Gachon University
1342 Seongnam-daro, Seongnam, S. Korea

Supporting information for this article is available on the WWW under <https://doi.org/10.1002/open.201900105>

©201x The Authors. Published by Wiley-VCH Verlag GmbH & Co. KGaA.
This is an open access article under the terms of the Creative Commons Attribution License, which permits use, distribution and reproduction in any medium, provided the original work is properly cited.

ferric oxide on a graphene aerogel for ORR, which outperformed over commercial Pt/C.^[22]

In this study, a manganese ferrite-decorated graphene aerogel ($\text{Mn}_x\text{Fe}_{3-x}\text{O}_4/\text{GAs}$) composite was synthesized by a reducing agent-assisted hydrothermal self-assembly process and was studied as a cathode material in a urea/ O_2 fuel cell. The structural and morphological properties of the $\text{Mn}_x\text{Fe}_{3-x}\text{O}_4/\text{GAs}$ catalyst were characterized. The electrochemical activity of the $\text{Mn}_x\text{Fe}_{3-x}\text{O}_4/\text{GAs}$ -modified electrodes were studied towards ORR using cyclic voltammetry and linear sweep voltammetry.

In addition, the performances of urea/ O_2 fuel cells comprising $\text{MnFe}_2\text{O}_4/\text{GAs}$ as a cathode material was evaluated.

2. Results and Discussion

2.1. Characterization of GO, MnFe_2O_4 , $\text{MnFe}_2\text{O}_4/\text{rGO}$, and $\text{MnFe}_2\text{O}_4/\text{GAs}$

The structures and crystallographic phases of graphene oxide (GO), MnFe_2O_4 , and $\text{MnFe}_2\text{O}_4/\text{GAs}$ particles were studied by XRD as plotted in Figure 1a. The pristine GO showed a characteristic

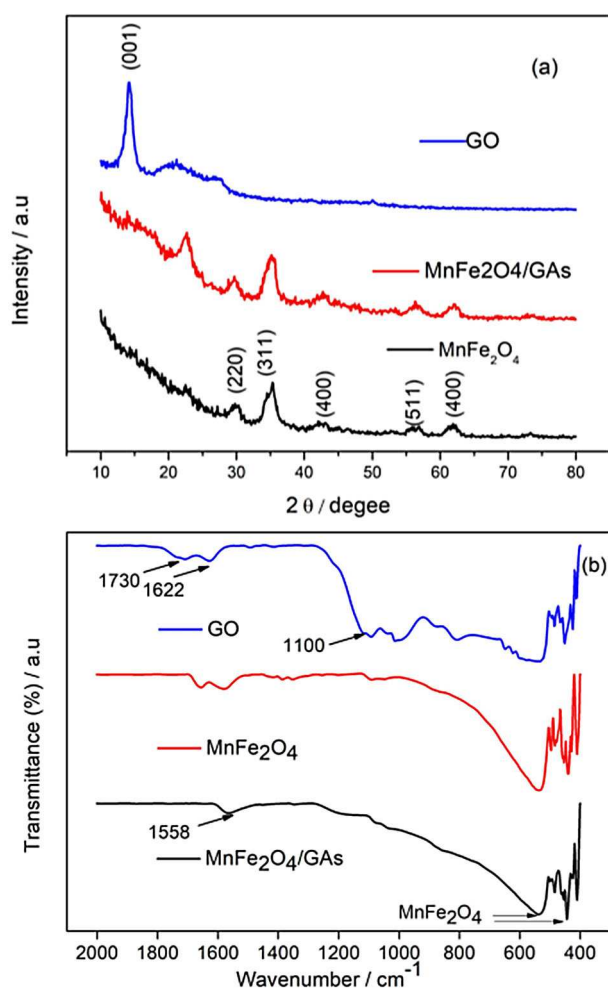


Figure 1. XRD patterns (a) and FTIR spectra (b) of GO, MnFe_2O_4 , and $\text{MnFe}_2\text{O}_4/\text{GAs}$.

reflection peak corresponding to the (001) plane. This peak originates from the inter planner spacing of graphene oxide due to the presence of different oxygenated functionalities on the surface. In the XRD pattern of $\text{MnFe}_2\text{O}_4/\text{GAs}$ (Figure 1a) and $\text{Mn}_{0.5}\text{Fe}_{2.5}\text{O}_4/\text{GAs}$ (Suppl. Figure S1), the disappearance of (001) reflection peak suggested the reduction of GO into graphene sheets. Additionally, in the diffraction spectrum of $\text{MnFe}_2\text{O}_4/\text{GAs}$, peaks corresponding to the diffraction planes viz., (220), (311), (400), (511), and (440) [JCPDS-10-0319]^[23] were also seen. Both $\text{MnFe}_2\text{O}_4/\text{GAs}$ and MnFe_2O_4 displayed similar diffraction pattern. The diffraction peaks of the two samples can be traced to a face-centered cubic crystal structure, indicating a phase pure synthesis of MnFe_2O_4 .

The functional groups in GO, MnFe_2O_4 , and $\text{MnFe}_2\text{O}_4/\text{GAs}$ were analyzed by FT-IR spectroscopy, as shown Figure 1b. The characteristic peaks of GO appeared at 1730 cm^{-1} (stretching vibration of C=O), 1622 cm^{-1} (skeletal stretching vibrations of C=C), and 1100 cm^{-1} (C–O stretching vibrations). On the other hand, for $\text{MnFe}_2\text{O}_4/\text{GAs}$, the characteristic peak of GO at 1730 cm^{-1} shifted to 1558 cm^{-1} , implying that the MnFe_2O_4 particles were strongly adsorbed onto the GO surface by chemical reduction.^[24–26] From the FTIR spectrum of $\text{MnFe}_2\text{O}_4/\text{GAs}$, the vibration peaks of the most oxygen-containing group disappeared, indicating that GO reduced during the hydrothermal and self-assembly processes; this agrees with the XRD result.^[27]

Figure 2 shows the SEM images and EDX elemental maps of $\text{MnFe}_2\text{O}_4/\text{GAs}$ and $\text{MnFe}_2\text{O}_4/\text{rGO}$. For $\text{MnFe}_2\text{O}_4/\text{GAs}$, a 3D

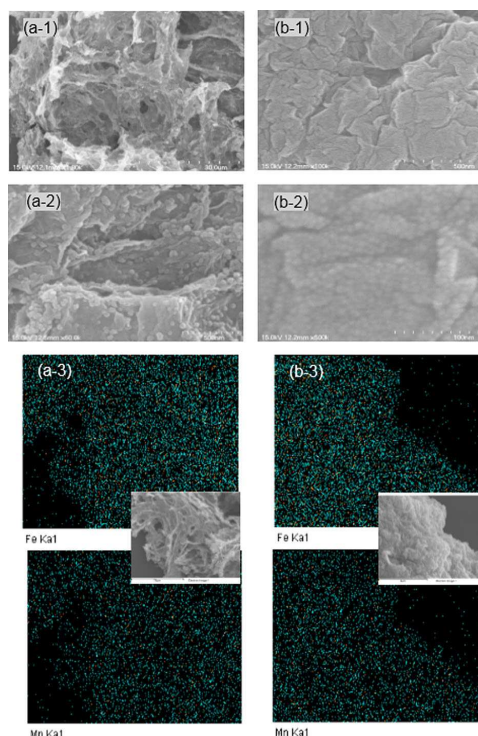


Figure 2. SEM images of $\text{MnFe}_2\text{O}_4/\text{GAs}$ (a-1, a-2) and $\text{MnFe}_2\text{O}_4/\text{rGO}$ (b-1, b-2), and EDX elemental maps corresponding to SEM images (a-3, b-3).

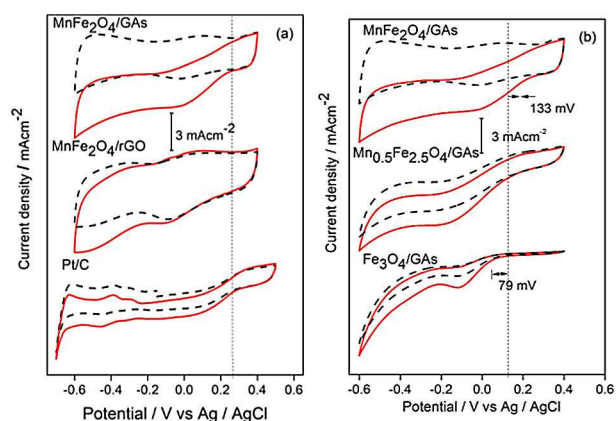


Figure 3. CV curves of $\text{MnFe}_2\text{O}_4/\text{GAs}$, $\text{MnFe}_2\text{O}_4/\text{rGO}$, and Pt/C (a) and $\text{Mn}_x\text{Fe}_{3-x}\text{O}_4/\text{GAs}$ (b) in O_2 (solid) and N_2 (dashed) saturated 0.1 M KOH electrolyte at a scan rate of 20 mVs^{-1} .

graphene aerogel framework with a continuous macroporous structure is clearly seen in Figure 2a. The graphene sheets were interconnected together forming a corrugated structures (Suppl. Figure S2). The MnFe_2O_4 nanoparticles were uniformly dispersed over the graphene aerogel matrix. On the other hand, the SEM images of $\text{MnFe}_2\text{O}_4/\text{rGO}$ exhibit uniform-sized MnFe_2O_4 nanoparticles formed on the graphene surface, as shown in Figure 2b. In addition, the elemental maps of both the catalysts revealed uniform distributions of Mn and Fe, and the elemental spectra showed that the Mn/Fe ratio was close to the theoretical loading ratio (Suppl. Figure S3).

The 3D-structured $\text{MnFe}_2\text{O}_4/\text{GAs}$ exhibited a high BET surface area of $169 \text{ m}^2\text{g}^{-1}$ with an average pore size of 3.6 nm, whereas $\text{MnFe}_2\text{O}_4/\text{rGO}$ had a BET surface area of $158 \text{ m}^2\text{g}^{-1}$ with an average pore size of 5.03 nm, as measured by nitrogen adsorption (Suppl. Figure S4). Catalyst pore sizes of 2–10 nm range is known to be preferable for electrochemical applications because not only do these pores increase the active reaction sites, they also decrease mass-transfer resistance.^[28] The nitrogen adsorption-desorption isotherms $\text{MnFe}_2\text{O}_4/\text{GAs}$ and $\text{MnFe}_2\text{O}_4/\text{rGO}$ were observed to be type IV (according to IUPAC classification), indicating the presence of mesopores,^[29] which was consistent with pore size analysis. These isotherms showed H3 hysteresis loops, suggesting that slit shaped pores were formed by the aggregation of nonuniform sized and/or shaped graphene nanosheets.

2.2. Electrocatalytic Properties of MnFe_2O_4 NPs, $\text{MnFe}_2\text{O}_4/\text{rGO}$, and $\text{MnFe}_2\text{O}_4/\text{GAs}$

The CV curves of $\text{MnFe}_2\text{O}_4/\text{rGO}$, $\text{MnFe}_2\text{O}_4/\text{GAs}$, and Pt/C obtained in O_2 - and N_2 -saturated 0.1 M KOH aqueous solution are shown in Figure 3a. The reduction peak potentials of $\text{MnFe}_2\text{O}_4/\text{GAs}$ and $\text{MnFe}_2\text{O}_4/\text{rGO}$ appeared at -0.01 V and -0.1 V , respectively, indicating a considerable positive potential shift from $\text{MnFe}_2\text{O}_4/\text{rGO}$ to $\text{MnFe}_2\text{O}_4/\text{GAs}$, and thus, a higher catalytic efficiency with a reduced overpotential of $\text{MnFe}_2\text{O}_4/\text{GAs}$.

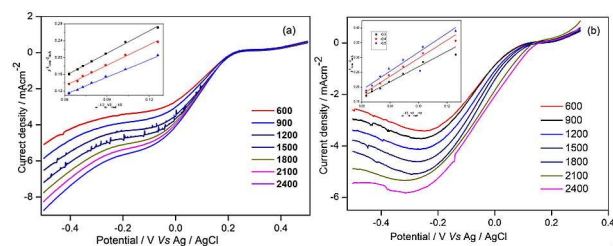


Figure 4. ORR polarization plots of $\text{MnFe}_2\text{O}_4/\text{GAs}$ (a) and $\text{MnFe}_2\text{O}_4/\text{rGO}$ (b) at different rpm in O_2 -saturated 0.1 M KOH (insets: Koutecky-Levich plots at different potentials) at a scan rate of 20 mVs^{-1} .

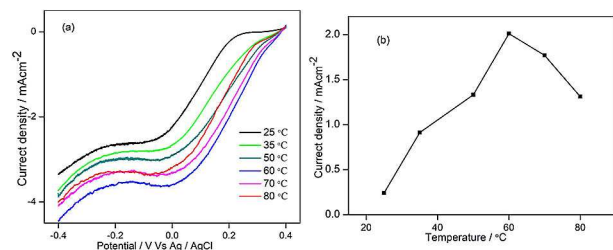


Figure 5. LSV of $\text{MnFe}_2\text{O}_4/\text{GAs}$ in O_2 saturated 0.1 M KOH at 900 rpm under different temperatures (a), and current density at 0.2 V vs temperature (b).

GAs for the ORR. In addition, ORR onset potentials of $\text{MnFe}_2\text{O}_4/\text{GAs}$ and commercial Pt/C appeared at a similar position, suggesting that the catalytic activity of $\text{MnFe}_2\text{O}_4/\text{GAs}$ is comparable with that of the Pt/C catalyst. In addition, the CV curves of $\text{Mn}_x\text{Fe}_{3-x}\text{O}_4/\text{GAs}$ with different x values are shown in Figure 3b. The results indicated that the presence of Mn oxide increased the ORR activity, mainly owing to the facilitation of the adsorption of oxygen by the corresponding redox of Mn oxide.^[17] Among the studied Fe/Mn ratios, the more positive ORR onset potential was observed for Fe/Mn = 2/1.

The ORR kinetics of the $\text{MnFe}_2\text{O}_4/\text{GAs}$ and $\text{MnFe}_2\text{O}_4/\text{rGO}$ catalysts were examined by rotating disc electrode (RDE) measurements with different electrode rotation rates. The half-wave potential of $\text{MnFe}_2\text{O}_4/\text{GAs}$ at 900 rpm was 0.09 V, which was shifted positively as compared to that of $\text{MnFe}_2\text{O}_4/\text{rGO}$ (-0.01 V), further indicating enhanced ORR activity of $\text{MnFe}_2\text{O}_4/\text{GAs}$ probably due to its 3D structure. The insets in Figure 4a and 4b show the Koutecky-Levich (K-L) plots at different potentials. The linearity and parallel profiles revealed that the ORR on the catalyst surface of the electrode occurred by the first-order kinetics and a similar number of electron transfer, respectively.^[18] From the slope of the K-L plots, the number of electrons transferred on the catalysts was estimated to be ~ 3.73 for $\text{MnFe}_2\text{O}_4/\text{rGO}$ and ~ 3.97 for $\text{MnFe}_2\text{O}_4/\text{GAs}$, suggesting a 4-e^- transfer process of ORR as similar to the 4-e^- process of ORR on Pt/C.^[2]

Figure 5a presents the ORR polarization curves of the $\text{MnFe}_2\text{O}_4/\text{GAs}$ catalyst at 900 rpm with different temperatures from 25 to 80°C . The current density measured at 0.2 V increased with temperature up to 60°C and then decreased, as shown in Figure 5b. According to Arrhenius equation, the ORR rate enhances with temperature. However, gaseous oxygen

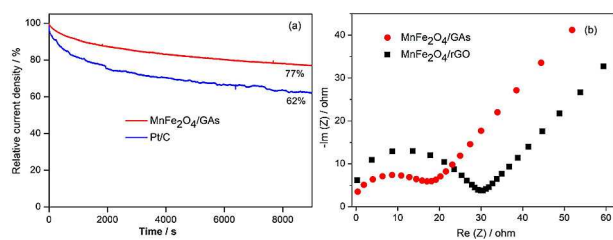


Figure 6. Chronoamperometric responses of $\text{MnFe}_2\text{O}_4/\text{GAs}$ and Pt/C in O_2 -saturated 0.1 M KOH at 0.1 V (a) and Nyquist plots of urea/ O_2 fuel cell with $\text{MnFe}_2\text{O}_4/\text{GAs}$ and $\text{MnFe}_2\text{O}_4/\text{rGO}$ cathode catalysts from 10 Hz to 5 MHz frequency.

needs to be dissolved in an aqueous KOH solution before it is used in the ORR; therefore, a high temperature adversely affected the ORR rate because the solubility of oxygen in water decreased with temperature.

The stabilities of $\text{MnFe}_2\text{O}_4/\text{GAs}$ and Pt/C were studied by chronoamperometric measurements at a constant potential of -0.1 V, as shown Figure 6a. The $\text{MnFe}_2\text{O}_4/\text{GAs}$ showed a slower current decay than the commercial Pt/C did. $\text{MnFe}_2\text{O}_4/\text{GAs}$ retained 77% of its initial current density after 150 min of continuous running. The deactivation of Pt/C in an alkaline solution is known to occur by the formation of Pt hydroxide on its surface.^[30]

Electrochemical impedance spectroscopy measurement was carried out to further examine ORR on both $\text{MnFe}_2\text{O}_4/\text{GAs}$ and $\text{MnFe}_2\text{O}_4/\text{rGO}$ catalysts, as shown in Figure 6b. From the Nyquist plots, the charge transfer resistance was estimated from the diameter of the semicircle. The charge transfer resistance of $\text{MnFe}_2\text{O}_4/\text{rGO}$ was $30.5 \Omega \text{ cm}^2$, and decreased to $17.5 \Omega \text{ cm}^2$ for $\text{MnFe}_2\text{O}_4/\text{GAs}$, further indicating that the $\text{MnFe}_2\text{O}_4/\text{GAs}$ catalyst exhibited better charge-transfer kinetics towards ORR.

2.3. Performances of uUea/ O_2 Fuel Cells with $\text{MnFe}_2\text{O}_4/\text{rGO}$ and $\text{MnFe}_2\text{O}_4/\text{GAs}$

Urea/ O_2 fuel cells were fabricated using $\text{MnFe}_2\text{O}_4/\text{rGO}$, $\text{MnFe}_2\text{O}_4/\text{GAs}$, and Pt/C as cathode materials, separately. The I - V polarization and power density curves of these cells with 0.33 M urea in 1.0 M KOH feed as an anolyte and dissolved O_2 bubbled as a catholyte at different temperatures are shown Figure 7. The best fuel cell performance was observed for the $\text{MnFe}_2\text{O}_4/\text{GAs}$ cathode catalyst, mainly because of its mesoporous 3D network structure with a high BET surface area, as discussed earlier. $\text{MnFe}_2\text{O}_4/\text{GAs}$ exhibited an OCV of 0.713 V and a maximum power density of 1.7 mW cm^{-2} at 60°C , which was even higher than that of commercial Pt/C .

3. Conclusions

Manganese ferrite decorated on a graphene aerogel was synthesized and studied as a cathode catalyst for a urea/ O_2 fuel cell. GO was reduced, and MnFe_2O_4 nanoparticles were

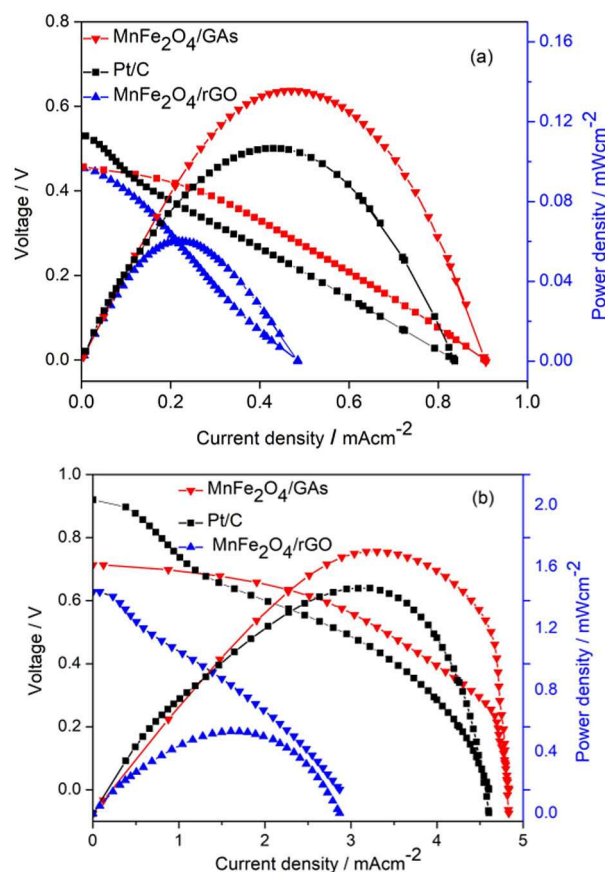


Figure 7. Performances of urea/ O_2 fuel cells with various cathode materials ($\text{MnFe}_2\text{O}_4/\text{rGO}$, $\text{MnFe}_2\text{O}_4/\text{GAs}$, and Pt/C) in 0.33 M urea in 1.0 M KOH as an anolyte and humidified O_2 as a catholyte at 25°C (a) and 60°C (b).

deposited on the highly porous 3D network-structured $\text{MnFe}_2\text{O}_4/\text{GAs}$ composite materials. The $\text{MnFe}_2\text{O}_4/\text{GAs}$ catalysts exhibited a distinct electrocatalytic activity toward ORR, which was higher than that of $\text{MnFe}_2\text{O}_4/\text{rGO}$, with an enhanced stability, possibly because of its mesoporous 3D network structure with a high BET surface area. The $\text{MnFe}_2\text{O}_4/\text{GAs}$ exhibited an OCV of 0.713 V and a maximum power density of 1.7 mW cm^{-2} at 60°C , which was even higher than that of the commercial Pt/C . The results demonstrated that the 3D structured graphene aerogel-supported MnFe_2O_4 can be a promising ORR catalyst.

Experimental Section

Synthesis of Graphene Oxide

Graphene oxide (GO) was synthesized from graphite flakes by a modified Hummers process.^[31] Briefly, 3.0 g of graphite flakes was added into 400 mL of concentrated $\text{H}_2\text{SO}_4/\text{H}_3\text{PO}_4$ (9:1). Then, 18 g of KMnO_4 (18.0 g) was added and stirred for 12 h at 50°C . After the reaction completed, it was cooled and poured into an ice water (400 mL) containing 6 mL of 30% H_2O_2 . The final product was centrifuged, washed to remove excess acid, and freeze-dried at -60°C for 72 h.

Synthesis of $Mn_xFe_{3-x}O_4$ -Decorated Graphene Aerogel

$Mn_xFe_{3-x}O_4$ was impregnated into a graphene aerogel using metal salts and GO as precursors and hydrazine monohydrate as a reducing agent.^[20] First, 140 mg of GO was dispersed in 90 mL of deionized (DI) water by sonication for 30 min. To this suspension, stoichiometric amounts of $Fe(Cl)_3 \cdot 6H_2O$ and $MnCl_2 \cdot 4H_2O$ were added (Suppl. Table S1). The mixture was neutralized using 5 M NaOH, followed by the addition of 2 mL of hydrazine monohydrate as a reducing agent and stirred continuously for 30 min. It was then transferred to a 100-mL autoclave reactor and kept at 180 °C under stationary condition for 12 h. The resulting black hydrogel was freeze-dried to obtain graphene aerogel-supported manganese ferrite oxides ($Mn_xFe_{3-x}O_4/GAs$).

$MnFe_2O_4$ nanoparticles ($MnFe_2O_4$ NPs) were also synthesized by reducing the precursor salts with hydrazine as described above. $MnFe_2O_4$ supported on reduced GO ($MnFe_2O_4/rGO$) was prepared by mixing $MnFe_2O_4$ NPs with GO suspension and reducing the mixture with hydrazine, as described elsewhere.^[32]

Preparation of Electrodes and Urea/ O_2 Fuel Cell Testing

The as-prepared $Mn_xFe_{3-x}O_4/GAs$ and $MnFe_2O_4/rGO$ catalyst powders and the commercial Pt/C (20%, E-TEK) powder were dispersed in 5% Nafion solution in isopropanol, respectively, and sonicated for 30 min. The resulting inks were coated on a glassy carbon electrode with a loading of $20 \mu g cm^{-2}$ and the electrochemical properties were measured. The catalyst ink was also coated on a 5.0-cm^2 carbon paper to prepare the cathode with a catalyst loading of $1 mg cm^{-2}$, and the anode was prepared using a commercial Ni/C (20%, E-Tek) with the same loading. An anion exchange membrane (AEM; Fumasep FAA-3-PK-130, Germany) was used as a polymer electrolyte separating the anode and cathode compartments. Membrane electrode assemblies (MEAs) for fuel cell tests were fabricated from both the electrodes and AEM by hot-pressing. A single-cell bipolar plate was set using graphite with serpentine flow channels. A urea solution of 0.33 M in 1 M KOH was pumped into the anode side by a peristaltic pump at $2 mL min^{-1}$, and humidified O_2 was supplied to the cathode.

Analysis

The crystallographic phases and structures of the samples were examined using an X-ray diffraction analyzer (XRD, Rigaku D/MAX-2002, Japan) with $Cu K\alpha$ radiation with a wavelength of 1.5406 \AA by scanning the samples in the 2θ range of 5° to 80° at a rate of $2^\circ min^{-1}$. The morphology of the samples was studied by scanning electron microscopy (SEM, Hitachi-4700, Japan). Functional groups in the powder were analyzed using a Fourier transform infrared (FTIR) spectrometer (Bruker, Saarbrücken, Germany). The Brunauer-Emmett-Teller (BET) surface area was measured from nitrogen adsorption and desorption isotherms, which were recorded at 77 K after degassing the analyte at 250 °C with a surface area analyzer (Micromeritics ASAP 2020, USA).

The ORR catalytic activities of the prepared samples were measured by cyclic voltammetry (CV), chronoamperometry (CA), and linear sweep voltammetry (LSV) by using a potentiostat (Biologic Sp-240) and a rotating ring disc electrode apparatus (RRDE-3A, ALS Company, Japan) with a three-electrode configuration. A glassy carbon-supported active material was used as the working electrode, Ag/AgCl filled with saturated KCl was used as the reference electrode, and Pt wire was used as the counter electrode. CV measurements were carried out with a supply of oxygen, while

background current was collected by bubbling nitrogen. All current densities were normalized to the respective surface areas.

Acknowledgements

This work was supported by the Basic Science Research Program through the National Research Foundation of Korea (NRF) funded by the Ministry of Education, Science and Technology (2017R1AB4002083).

Conflict of Interest

The authors declare no conflict of interest.

Keywords: oxygen reduction reaction · urea fuel cell · anode catalyst · manganese ferrite · graphene aerogel

- [1] R. Jiang, D. Chu in *Non-Noble Met. Fuel Cell Catal* (Eds.: Z. Chen, J.-P. I Dodelet, J. Zhang), Wiley-VCH, Weinheim **2014**, pp 271–318.
- [2] U. Krewer, C. Weinzierl, N. Ziv, D. R. Dekel, *Electrochim. Acta* **2018**, *263*, 433–446.
- [3] E. C. Serban, A. Balan, A. M. Iordache, A. Cucu, C. Ceaus, M. Necula, G. Ruxanda, C. Bacu, E. Mamut, I. Stamatin, *Dig. J. Nanomater. Biostructures* **2014**, *9*, 1647–1654.
- [4] D. R. Dekel, *J. Power Sources* **2018**, *375*, 158–169.
- [5] P. A. Christensen, A. Hamnett, D. Linares-Moya, *Phys. Chem. Chem. Phys.* **2011**, *13*, 5206–5214.
- [6] J. K. Nørskov, J. Rossmeisl, A. Logadottir, L. Lindqvist, D. Lyngby, H. Jo, *J. Phys. Chem.* **2014**, *108*, 17886–17892.
- [7] J. Li, A. Alsudairi, Z. F. Ma, S. Mukerjee, Q. Jia, *J. Am. Chem. Soc.* **2017**, *139*, 1384–1387.
- [8] Y. Liang, H. Wang, J. Zhou, Y. Li, J. Wang, T. Regier, H. Dai, *J. Am. Chem. Soc.* **2012**, *134*, 3517–3523.
- [9] M. Liu, Y. Dong, Y. Wu, H. Feng, J. Li, *Chem. Eur. J.* **2013**, *19*, 14781–14786.
- [10] N. Mahmood, C. Zhang, J. Jiang, F. Liu, Y. Hou, *Chem. Eur. J.* **2013**, *19*, 5183–5190.
- [11] B. Anasori, M. Beidaghi, Y. Gogotsi, *Mater. Today* **2014**, *17*, 253–254.
- [12] H. Zhu, S. Zhang, Y. X. Huang, L. Wu, S. Sun, *Nano Lett.* **2013**, *13*, 2947–2951.
- [13] K. V. Sankar, R. K. Selvan, *RSC Adv.* **2014**, *4*, 17555–17566.
- [14] S. Khilari, S. Pandit, J. L. Varanasi, D. Das, D. Pradhan, *ACS Appl. Mater. Interfaces* **2015**, *7*, 20657–20666.
- [15] Y. Zou, Y. Wang, *ACS Nano* **2011**, *5*, 8108–8114.
- [16] J. Feng, Y. Liang, H. Wang, Y. Li, B. Zhang, J. Zhou, J. Wang, T. Regier, H. Dai, *Nano Res.* **2012**, *5*, 718–725.
- [17] C. H. Choi, S. H. Park, S. I. Woo, *Phys. Chem. Chem. Phys.* **2012**, *14*, 6842–6848.
- [18] J. Xiao, Q. Kuang, S. Yang, F. Xiao, S. Wang, L. Guo, *Sci. Rep.* **2013**, *3*, 1–8.
- [19] X. Yao, Y. Zhao, *Chem.* **2017**, *2*, 171–200.
- [20] L. Ren, K. S. Hui, K. N. Hui, *J. Mater. Chem. A.* **2013**, *1*, 5689–5694.
- [21] Z. Fan, D. Z. Y. Tng, C. X. T. Lim, P. Liu, S. T. Nguyen, P. Xiao, A. Marconnet, C. Y. H. Lim, H. M. Duong, *Colloids Surf. A Physicochem. Eng. Asp.* **2014**, *445*, 48–53.
- [22] Z. Wu, S. Yang, Y. Sun, K. Parvez, X. Feng, *J. Am. Chem. Soc.* **2012**, *134*, 9082–9085.
- [23] M. Y. Rafique, P. Li-qing, Q. Javed, M. Z. Iqbal, *Chin. Phys. B.* **2013**, *22*, 17101–17107.
- [24] W. Chen, S. Li, C. Chen, L. Yan, *Adv. Mater.* **2011**, *23*, 5679–5683.
- [25] K. V. Sankar, R. K. Selvan, *J. Power Sources.* **2015**, *275*, 399–407.
- [26] G. Wang, Y. Ma, Z. Wei, M. Qi, *Chem. Eng. J.* **2016**, *289*, 150–160.
- [27] N. Ueda Yamaguchi, R. Bergamasco, S. Hamoudi, *Chem. Eng. J.* **2016**, *295*, 391–402.
- [28] W. Li, J. Liu, D. Zhao, *Nat. Rev. Mater.* **2016**, *1*, 16023.

- [29] G. Leofanti, M. Padovan, G. Tozzola, B. Venturelli, Surface area and pore texture of catalysts. *Catal. Today* **1998**, *41*, 207–219.
- [30] J. Greeley, I.E.L. Stephens, A.S. Bondarenko, T.P. Johansson, H.A. Hansen, T.F. Jaramillo, J. Rossmeisl, I. Chorkendorff, J.K. Nørskov, *Nat. Chem.* **2009**, *1*, 552–556.
- [31] D.C. Marcano, D.V. Kosynkin, J.M. Berlin, A. Sinitskij, Z. Sun, A. Slesarev, L.B. Alemany, W. Lu, J.M. Tour, *ACS Nano*. **2010**, *4*, 4806–4814.
- [32] Y. Xiao, X. Li, J. Zai, K. Wang, Y. Gong, B. Li, Q. Han, X. Qian, *Nano-Micro Lett.* **2014**, *6*, 307–315.

Manuscript received: March 25, 2019